Volume 1 | Number 1 | Jan 2013 | Pages 1–100

PCCP

Physical Chemistry Chemical Physics
www.rsc.org/pccp

ROYAL SOCIETY OF CHEMISTRY

ROYAL SOCIETY OF CHEMISTRY

www.rsc.org/pccp

The Role of Chemisorbed Hydroxyl Species in Alkaline Electrocatalysis of Glycerol on Gold[†]

X. Shi, D. E. Simpson and D. Roy[*]

Department of Physics, Clarkson University, Potsdam,
New York 13699-5820, U.S.A

Abstract. The mechanism of energy conversion in a direct glycerol fuel cell (DGFC) is governed by the anode-supported heterogeneous steps of glycerol electro-oxidation. In aerated alkaline electrolytes, glycerol also participates in a base catalyzed process, which can release certain species mixing with the anode catalyzed surface products. As a result, selective probing of the surface catalytic reactions involving such systems can be difficult. The present work addresses this issue for a gold anode by using the analytical capability of cyclic voltammetry (CV). In addition, surface plasmon resonance measurements are used to optically probe the adsorption characteristics of the electrolyte species. The net exchange current of the oxidation process and the transfer coefficient of the rate determining step are evaluated by analyzing the CV data. The interfacial reactions and their products on Au are identified by measuring the number of electrons released during the electro-oxidation of glycerol. The results indicate that these reactions are facilitated by the surface bound hydroxyl species on Au (chemisorbed OH^- and faradaically formed Au-OH). By comparing the findings for stationary and rotating electrodes, it is shown that, convective mass transport is critical to maintaining efficient progression of the consecutive oxidation steps of glycerol. In the absence of hydrodynamic support, the main surface products of glycerol oxidation appear to be glyceraldehyde, glycerate and malonate, formed through a net six-electron route. In the presence of controlled convection, a ten-electron process is activated, where mesaxolate is the likely additional product.

[†] Electronic supplementary information (ESI) available.
[*] E-mail: samoy@clarkson.edu

1. Introduction

Glycerol (Gly) is readily available as a derivative of biodiesel, and even in its crude form, can serve as a cost effective fuel for direct glycerol fuel cells (DGFCs). This utility of Gly is largely governed by the efficiency of its electro-catalytic oxidation at the anode surface of the fuel cell. While Pd and Pt (as well as their composites) are frequently used as catalysts for Gly oxidation,[1-3] the performance of Au for this application in alkaline solutions is also widely recognized.[4, 5] Specifically, a polycrystalline Au electrode can often function as a more efficient electrocatalyst for Gly oxidation as compared to polycrystalline Pt and Pd electrodes.[4] This catalytic function of Au is generally associated with the reaction sites of surface bound hydroxyl species that typically exist in alkaline solutions as incipient hydrous oxides (IHOs).[6-8] However, in the specific case of glycerol oxidation on Au, the detailed mechanisms of IHO-mediated electrocatalysis as well as their accompanying features of convective mass transfer have remained fairly underexplored.

Low-coordination ad-atoms on a metal surface constitute the sites of IHO formation where the local activation energies of heterogeneous reactions are reduced.[7, 9] The IHO forms under moderate anodic activation, before the main oxide species is generated; this frequently involves the adsorption of a single OH^- ion, which, depending on the surface potential, may be partially discharged.[10, 11] This adsorbed species becomes readily available for anodic reactions that require the surface-localized hydroxyl as a reactant. The fardaic process supported in this way is manifested as an electrocatalytic (low overpotential) reaction. Using polycrystalline and thin-film Au electrodes under hydrodynamic control in alkaline electrolytes, we examine here the implications of such a mechanism in the electro-oxidation of Gly on Au.

Two parallel groups of experiments are performed here using a Gly-free reference (Ref.) solution of 2 M NaOH and a set of Gly-added (0.03 or 1.0 M) electrolytes. The considerations for choosing these electrolyte concentrations are discussed in the Electronic Supporting Information (ESI) accompanying this report. Cyclic voltammetry (CV) is employed as a comprehensive diagnostic probe of the surface reactions. Scan rate dependent CV is used with a thin-film and a polycrystalline Au electrode to examine the reaction kinetics under stationary conditions. A rotating disc electrode (RDE) is employed to examine how the total charge-yield of Gly oxidation is affected by convection controlled transfer of surface reactants. The relative functions of the co-adsorbing surface species are checked optically by using angle-resolved surface plasmon resonance (SPR) measurements. Certain theoretical considerations of data analysis for the electrochemical measurements are summarized in the next section, followed by a brief Experimental section. The results presented in the subsequent sections demonstrate how the CV and the SPR methods can be effectively combined to study the electrocatalytic reactions on Au.

2. Theoretical considerations

2.1. Scan rate controlled voltammetry as a probe of multistep electrochemical reactions

Electro-oxidation of Gly typically proceeds through a multistep sequence of reactions,[1-5] and scan rate dependent CV can serve as a useful analytical probe of such reactions. The present work uses this approach to examine the reaction kinetics of Gly on stationary Au electrodes where convective transport of reactants is absent. The analysis of these CV data is based here on a generalized Butler Volmer formulation of multi-step faradaic reactions. The detailed theoretical

aspects of this topic have been discussed by previous authors,[12-14] and only certain essential points related to the present investigation are briefly outlined here.

The main assumptions of the theoretical formulation adopted in this work are as follows:[13] (i) The forward and backward reactions have the same rate determining step (RDS) and occur in a steady state; (ii) the electrode surface does not contain any passive regions; and (iii) the stoichiometric number associated with the RDS is 1 (which typically is the case, except for complex reactions such as those involving polymerization of reaction products). The electrode current density described according to these considerations under kinetic control has the following form:[12] $i_k = i_{ka} - i_{kc}$, where i_{ka} and i_{kc} are the anodic and cathodic components of i_k, respectively; $i_{ka} = i_0 \exp[\beta_a F \eta / (RT)]$; $i_{kc} = i_0 \exp[(-\beta_c F \eta)/(RT)]$. i_0 is an effective exchange current, which depends on the rate constants of all the intermediate reaction steps.[14] F, R and T denote the Faraday constant, gas constant and temperature, respectively. η is the activation overpotential; $\eta = E - E_0$; E is the applied voltage; E_0 is the null potential; β_a and β_c are the anodic and cathodic transfer coefficients, respectively.

The total number of electrons (n) transferred in the multi-step process is: $n = n_1 + n_a + n_2$, where n_1 and n_2 are the numbers of single electron steps occurring before and after the RDS, respectively; n_a is the number of electrons linked to the RDS. In addition, $\beta_a = n_1 + n_a(1-\alpha)$, $\beta_c = n_2 + n_a\alpha$, α is the symmetry factor of the RDS, and $\beta_a + \beta_c = n$.[12, 13] If the RDS is the first step of the multi-step process ($n_1 = 0$) then the transfer coefficient of the overall forward reaction simplifies as $\beta_a = n_a(1-\alpha)$. Under this condition, and if the given faradaic reaction is irreversible in the cathodic direction, then:

$$i_k \approx i_{ka} = i_0 \exp\left[\frac{n_a(1-\alpha)F\eta}{RT}\right], \tag{1}$$

where all steps of the reaction are kinetically controlled.

In the presence of diffusional transport in the RDS, the following form of the electrode current density (i) can be used for simple calculations on the basis of phenomenological considerations: $i = i_k[c_a(t,x=0)/c_a(t,x=\infty)]$.[15] Here, t denotes time in a CV scan; $x=0$ is the coordinate of the electrode surface along the x direction (normal to the electrode extending into the electrolyte), and c_a is the concentration of the reactant involved in the RDS. If the multistep process begins with its RDS, then it is reasonable to assume that, $c_a(x=\infty)=c_b$, and $c_a(x=0)=c(0)$, where $c(0)$ and c_b are the interfacial and bulk concentrations of the initial reactant, respectively. By incorporating these concentration terms [along with i_k from eqn (1)] in the above expression of i, and by using the result in Fick's law, the electrode current can be written in the same form as that commonly used to describe single-step irreversible faradaic reactions.[16] In this formalism, the following expression is obtained for the voltammetric anodic peak current (i_p):[15]

$$i_p = 2.99 \times 10^5 (nc_b)[(1-\alpha)n_a Dv]^{1/2} \tag{2}$$

where v denotes the voltage scan rate of CV, and D is the diffusion coefficient of the reactant governing the RDS. The voltage (E_p) corresponding to this peak current is written as[16-18]

$$E_p = E^{0/} + E_{p0} + \frac{RT}{(1-\alpha)n_a F}\ln\left[\frac{(1-\alpha)n_a Fv}{RT}\right]^{1/2} \tag{3}$$

where $E^{0/}$ is the formal potential of RDS. $E_{p0} = [RT/\{(1-\alpha)n_a F\}][0.78+\ln(\sqrt{D}/k_s^0)]$, and k_s^0 denotes the rate constant of the RDS. According to eqns (2) and (3), the kinetic parameters,

α, n_a and n, can be obtained from scan rate dependent CV data, by analyzing the linear correlations of the parameters combined in the [E_p vs. (ln v)] and the [i_p vs. $\sqrt{v}$] pairs.[17, 18]

2.2. RDE voltammetry as a probe of multistep electrochemical reactions

RDE voltammetry has been employed in this study to examine the reaction kinetics of Gly oxidation in the presence of convective mass transport. In general, the current-voltage characteristic of an irreversible multistep reaction occurring at the surface of an RDE can be expressed using the Koutecký–Levich equation: $(1/i) = (1/i_L) + (1/i_k)$, where, i_L is the limiting current. In the present context i_k is defined by eqn (1), and hence the Koutecký–Levich equation takes the form:

$$\ln\left(\frac{i}{i_L - i}\right) = \ln\left(\frac{i_0}{i_L}\right) + \frac{(1-\alpha)n_a F\eta}{RT} \tag{4}$$

which corresponds to the general form of the Tafel equation, with the mass transfer controlled current contributions resolved in the i_L term. The limiting current is activated at a high overpotential, where $c(0) \to 0$, and $i \to i_L = (nFDc_b)/\delta_0$, with δ_0 denoting the Nernst diffusion layer thickness. Under steady state conditions, i_L is defined by the Levich equation[15],

$$i_L = 0.62nFD^{2/3}\omega^{1/2}c_b v_e^{-1/6} \tag{5}$$

which corresponds to $\delta_0 = 1.61D^{1/3}v_e^{1/6}\omega^{-1/2}$, with v_e and ω denoting the viscosity of the electrolyte and the electrode rotation speed, respectively.

To determine n from RDE experiments, it is necessary to perform quasi steady state CV at different speeds of disc rotation.[19] The values of i_L measured from these experiments can be plotted against $\omega^{1/2}$ to obtain linear Levich plots according to eqn (5), and the value of n can be

evaluated from the resulting slopes of these plots. The results can be further checked by using Koutecký–Levich (i^{-1} vs. $\omega^{-1/2}$) plots, the linear slopes of which would also give the value of n.[20] This analysis can also be used to extract the RDS parameter, α, which can be compared with the corresponding result for stationary electrodes; such comparisons could indicate the role of hydrodynamic control in governing the RDS.

3. Experimental Section

Aqueous solutions of 2M NaOH (Fishier Scientific) with and without Gly (ultrapure, Alfa Aesar) were prepared with triply distilled water. The polycrystalline stationary working electrode was a gold rod (99.99% pure, 6.35 mm diameter, from Alfa Aesar) inserted in a Teflon holder with only a flat surface exposed to the electrolyte. An identical electrode sample was also mounted on the RDE holder, and the RDE was controlled by a Pine Instruments AFMSRX rotator. The active sample areas exposed to the electrolyte were 1.49, 0.32 cm^2 for the thin film and the polycrystalline electrodes, respectively. The film electrode (from Gentel Bioscienes) consisted of a thin layer (47.5 nm) of Au, deposited on an SF-10 glass slide, via an intermediate (2.92 nm thick) Cr binder layer.

CV experiments were performed at room temperature in a standard three-electrode cell (of glass or Teflon body, and controlled by a VersaSTAT3 potentiostat), by employing a saturated calomel electrode (SCE) reference and a Pt wire counter electrode. Angle resolved SPR data were collected by using a standard attenuated total reflection geometry based on the Kretschmann configuration with p-polarized diode laser light at the 636 nm wavelength.[21] Further experimental details of the present work are presented in the ESI.

4. Results and Discussion

4.1. Voltammetry of thin film and polycrystalline stationary Au electrodes in the reference electrolyte of NaOH

Fig. 1A shows CV data for a gold film electrode, recorded at a scan rate of 50 mV s^{-1}. The weak anodic current feature a_1 observed at ~0 V in Fig. 1A corresponds to the reaction,[10]

$$Au + OH^- = Au(OH)_{ad}^{\delta-} + \lambda e^- \tag{6}$$

where $Au(OH)_{ad}^{\delta-}$ is the IHO of Au with "ad" denoting adsorbed species. λ is the voltage dependent partial charge transfer coefficient; $0 \le \lambda \le 1$ and $\delta = (1-\lambda)$.[22] The current peak a_2 represents the reaction: $Au(OH)_{ad}^{\delta-} + (x-1)OH^- = Au(OH)_x + (x-\lambda)e^-$, where $x \approx 3$ for strong alkaline solutions.[23] The cathodic current peaks c_1 and c_2 represent reduction of the oxidized species formed at a_1 and a_2, respectively. $Au(OH)_x$ oxidizes to AuO at 0.4 V, leading to the rising anodic current observed at the upper end of voltage scan.[10, 24]

Fig. 1B shows voltammograms for the Au film in 2 M NaOH, with v varied between 0.03 (inner most plot) and 1 V s^{-1}(outer most plot). As v is increased, both the anodic and the cathodic currents increase, and the weak current peaks, a_1 and c_1, merge with their adjacent larger peaks. The potentials (E_p) and the currents (i_p) of these merged voltammetric peaks are plotted as functions of log (v) and v in Fig. 1C and D, respectively. The characteristic features of E_p and i_p for the Ref. electrolyte do not follow the description of eqns (2) and (3) considered for Gly oxidation; instead, these parameters of Au oxidation are described by a different set of kinetic equations reported by Srinivasan and Gileadi.[25] The two E_p vs. [log (v)] plots in Fig. 1C are nearly parallel to the [log (v)] axis. These low-slope linear plots are typical of quasi-equilibrium

adsorption reactions where $E_p \approx (RT/F)\ln(k_{1b}/k_{1f})$, with k_{1f} and k_{1b} denoting the rate constants of the forward and reverse steps of Au hydroxide formation, respectively.[25]

The linear trends of the i_p plots seen in Fig. 1D are consistent with the aforementioned quasi-reversible reaction kinetics. According to model calculated results for such systems, $i_p = (Q_0 F/4RT)v$, where Q_0 is the charge-equivalent of a monolayer adsorption of OH^-.[25] Based on the above expression of i_p, the measured slope of the linear plot obtained in the anodic cycle of Fig. 1D gives $Q_0 = 0.22$ mC cm^{-2}. This value is in close agreement with the previously measured charge (0.21 mC cm^{-2}) for a monolayer electrosorption of OH^- on Au,[26] and suggests that reaction (6) likely serves as a first step in the formation of $Au(OH)_x$. The faradaic charge integrated under the anodic portion of the plot in Fig. 1A is 0.84 mC cm^{-2}, which corresponds to 3.9 monolayer-equivalent of $Au(OH)_{ad}$.

Fig. 2 shows the results of CV experiments performed with a stationary Au polycrystalline electrode. The overall features of these data are essentially the same as those seen in Fig. 1. Owing to the relatively higher spatial inhomogeneity of the polycrystalline surface sites,[27] the current peaks in Fig. 2A and B are broader than their counterparts in Fig. 1A and B. As a result, the a_1 feature is effectively masked in Fig. 2A. The slope of the i_p vs. v plots in Fig. 2D for the anodic formation of $Au(OH)_x$ corresponds to a value of Q_0 that is 2.65 times larger than that found for the thin-film electrode in Fig. 1D. This number is the approximate roughness factor of the polycrystalline Au surface as compared to that of the Au thin-film.[27] The integrated anodic charge (0.39 mC cm^{-2}) obtained from Fig. 2A suggests that, the $Au(OH)_x$ deposited on the polycrystalline Au surface is equivalent to 4.6 monolayers of $Au(OH)_{ad}$.

4.2. Cyclic voltammetry of thin film and polycrystalline stationary electrodes in the glycerol-added electrolyte of NaOH

Fig. 3A shows scan rate dependent CV data for the Au film electrode in 2 M NaOH + 0.1 M Gly. The peak shaped anodic currents are caused by electro-oxidation of Gly, and grow systematically with increasing values of v. Moreover, the current profile of the voltammogram in each anodic sweep is dominated by a single peak, which, in view of eqns (2) and (3) indicates a leading role of the RDS in the activation of Gly electro-oxidation. Since the electrode currents become negligible at $E < -0.5$ V, the cathodic bound of the CV scans was kept at this cut-off potential. The oxidation current peak shifts with variations in the voltage scan rate, but consistently occurs within a region of relatively low potentials between 0.2 and 0.5 V, and this moderate activation voltage of Gly oxidation signifies the electro-catalytic attribute of this reaction. AuO begins to form above 0.4V, and since this oxide is ineffective for supporting electro-oxidation of Gly, the anodic currents in Fig. 3A decrease to their baseline values in the corresponding voltage region. The irreversible nature of Gly oxidation is manifested in the recurrence of the anodic current peaks during the cathodic voltage scans.

The currents measured in the cathodic CV scans in Fig. 3A are a net result of Gly oxidation and gold-oxide reduction. The anodically formed gold oxide is reduced to regenerate the Gly oxidation current in the cathodic sweep. Moreover, at the end of the oxidation scan, the interfacial concentration of Gly drops due to mass transfer limitation,[28] and the reaction front may also become partially blocked by stagnant intermediates. As a combined result of these effects, the Gly oxidation currents observed during the cathodic CV sweeps are smaller than their counterparts recorded during the preceding anodic scans.

In a full-cell configuration of an alkaline DGFC, the complete oxidation of Gly ($C_3H_8O_3$) at the anode would involve a fourteen-electron process: $C_3H_8O_3 + 20OH^- = 3CO_3^{2-} + 14H_2O + 14e^-$. This reaction would be balanced by oxygen reduction at the counter electrode: $(7/2) O_2 + 7H_2O + 14e^- = 14OH^-$, with the total cell reaction expressed as: $C_3H_8O_3 + 6OH^- + (7/2) O_2 = 3CO_3^{2-} + 7H_2O$. Incomplete oxidation of Gly results in a net transfer of <14 electrons, which is the situation often encountered in half-cell measurements using unstirred electrolytes. The number of electrons (n) involved in the Gly oxidation reaction examined in Fig. 3 can be determined by analyzing the v dependent behaviors of the anodic peaks.[17]

The symbols in Fig. 3B and C denote, respectively, the experimental data for E_p and i_p taken from Fig. 3A. Considering that the voltammograms may contain some distorting features of the solution resistance (R_s), the E_p values were corrected for this effect. The linear fits to the data (symbols) in Fig. 3B and C are based on eqns (3) and (2), respectively. Since these equations are incorporated here according to the condition, $c_a(\infty) = c_b$, the existence of this condition in the present system is manifested in the correspondingly matched linear signatures of the peak parameters in Fig. 3. In other words, the observed trends of $E_p(v)$ and $i_p(v)$ provide further indication that, the initial step of Gly dehydrogenation is the RDS of Gly electro-oxidation on Au[29] and that, C_b is the bulk concentration of Gly in the experimental solution.

In Fig. 3B, the measured slope (indicated in the Figure) of the linear plot defined by eqn (3) is equal to $RT/[2(1-\alpha)n_aF]$, which corresponds to $n_a(1-\alpha)=0.11$. The linear slope of the plot in Fig. 3C according to eqn (2) is expressed as: $2.99\times10^5(nC_b)[(1-\alpha)n_aD]^{1/2}$. By combining the latter quantity with the aforementioned result for $n_a(1-\alpha)$, and by using the known values of c_b (taken as [Gly]) and D (diffusion coefficient of Gly in water at 25 ^{o}C,[30]

0.898×10^{-5} cm^2 s^{-1})[30], we obtain $n = 4.84$. The voltammograms shown in Fig. 4A for the polycrystalline Au electrode are similar to those shown in Fig. 3A. The (solution resistance corrected) peak currents and potentials observed in Fig. 4A are plotted in Fig. 4B and C, respectively. The scan rate dependencies of these E_p and i_p are similar to the corresponding peak parameters shown in Fig. 3 for the film electrode. The linear slope of the plot in Fig. 4B gives $n_a(1-\alpha) = 0.17$. By combining this value with the slope of the plot in Fig. 4C, we obtain $n = 4.32$ for the stationary polycrystalline Au electrode.

In both Figs. 3A and 4A, the anodic voltage corresponding to the flattening of the post-peak oxidation current shifts to higher values with increasing values of v. This suggests the presence of mass transport limited depletion of interfacial reactants, the onset of which is determined by the cumulative amount of faradaic charges generated during Gly oxidation.[28] Thus, the Gly oxidation currents are terminated at higher anodic potentials during the faster voltage scans. The anodic formation of AuO, a second factor responsible for ceasing Gly$^-$ oxidation during the anodic scans, may also play a role in determining the critical anodic voltage where the oxidation current stops.[10] Since the values of n evaluated from Figs. 3 and 4 are mutually comparable, it is evident that, the different surface roughness factors of the two types of Au electrodes in these two cases do not have significant effects on the mechanisms of Gly oxidation.

4.3. Synergistic roles of surface-bound OH and solution pH

It is known that the surface bound OH species of Au, identified here as $Au(OH)_{ad}^{\delta-}$,[24, 26] acts as a catalyst for alkaline oxidation of Gly (and other alcohols) by lowering the activation energy of dehydrogenation.[5, 31-34] To examine the present data in the framework of this mechanism, we

note that in alkaline solutions, chemisorption of OH^- on Au during an anodic scan generally starts at -0.4 V.[35] The surface coverage of the adsorbed OH^- increases almost linearly in the anodic direction up to ~0.2 V, until the Au surface begins to oxidize. Thus in the Ref. electrolyte, eqn (6) remains applicable within the -0.3 to 0.8 V range, where Gly oxidizes. Here, $\lambda \approx 0$ at $-0.3 \leq E \leq 0$ V, and $\lambda \approx 1$ in the voltage region of peak a_1 ($0 \leq E \leq 0.2\,V$),[26] and this maximum value of λ is maintained in the Au $(OH)_x$ regime if the latter species forms through layered growth of $Au(OH)_{ad}^{\delta-}$.

Since the voltage region of Gly oxidation overlaps with that of Au hydroxide formation, the $(OH)_{ad}^{\delta-}$ species affects the surface reactions of Gly.[5, 36, 37] According to the commonly accepted mechanism of this process, the oxidizing molecule from the solution anchors to the surface bound $(OH)_{ad}^{\delta-}$ site, and loses a hydrogen from the CH or CH_2 group.[5, 38] The Au site, initially occupied by the $(OH)_{ad}$, is regenerated and consumed again by reaction (6) to continue promoting the successive steps of Gly dehydrogenation. The consumption of $Au(OH)_{ad}^{\delta-}$ by Gly suppresses the generation of $Au(OH)_x$ from the IHO; this in turn weakens or eliminates the cathodic peak c_1 of $Au(OH)x$ reduction. The first step of Gly electrocatalysis in the above description has the form:

$$C_3H_8O_3 + Au(OH)_{ad}^{\delta-} + OH^- = Au + C_3H_6O_3 + 2H_2O + (1+\delta)e^- \qquad (7)$$

where $\delta \approx 0$ within the potential region of Gly oxidation.[26] The glyceraldehyde ($C_3H_6O_3$) produced by reaction (7) participates in the subsequent oxidation step.

Owing to the requirements of steric compatibility with bulk water, the OH groups of the Gly molecule considered in eqn (7) remain more hydrated than the CH/CH_2 groups, and orient toward the bulk electrolyte during adsorption.[37] This provides a favorable configuration for the

Gly molecule to adsorb with its weakly hydrated CH group anchoring at the $Au(OH)_{ad}^{\delta-}$ site, and consequently facilitates the dehydrogenation step (7). The essential role of the alkaline medium in this process is evident in the high-pH condition necessary to form/sustain the $Au(OH)_{ad}$ active sites through reaction (6). The net step of reactions (6) and (7) can be written as:

$$C_3H_8O_3 + Au + 2OH^- = C_3H_6O_3 + Au + 2H_2O + 2e^- \tag{8}$$
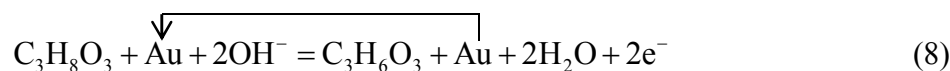
where the Au sites explicitly shown on the left and right hand sides of eqn (8) represent the catalytically "active" and "regenerated" sites, respectively.

The alkaline background solution plays a further role as a base-catalyst when its pH approaches the pK$_a$ of Gly, 14.15.[5, 39, 40] The pH value of the Gly added NaOH electrolytes used in this work was measured as 13.6, sufficiently close to the pKa of Gly to activate a measurable component of base catalysis. In the alkaline environment, Gly deprotonates as glycerolate (Gly$^-$ or $C_3H_7O_3^-$):

$$C_3H_8O_3 + OH^- \qquad C_3H_7O_3^- + H_2O \tag{9}$$
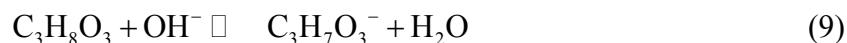
which is a solution-phase reaction.[41] According to eqn (9) and for the given pKa of Gly, about 20% of the Gly should exist as deprotonated Gly$^-$ in the experimental solution. This anion can be electro-oxidized to glyceraldehyde ($C_3H_6O_3$) through a single-electron step in a surface-catalyzed mechanism similar to that of reaction (7):[5]

$$C_3H_7O_3^- + Au(OH)_{ad}^{\delta-} = C_3H_6O_3 + H_2O + Au + (1+\delta)e^- \tag{10}$$
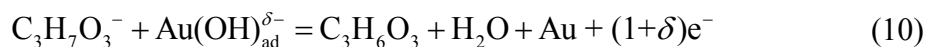
so that eqns (6) and (10) represent two sequential steps of the oxidation of glycerolate to glyceraldehyde. The net reaction is obtained by adding these two equations:
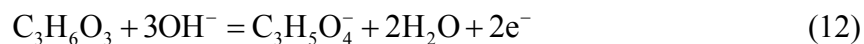
$$Au + OH^- + C_3H_7O_3^- = Au + C_3H_6O_3 + H_2O + 2e^- \tag{11}$$

14
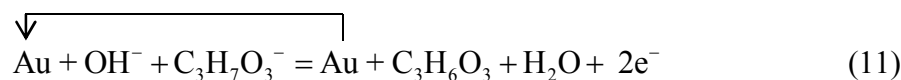
where the catalytic role of the Au site is underscored again with its inclusion on both sides of the resulting equation. Since Gly^- is more reactive than its protonated Gly form, reaction (11) can occur at a rather low overpotential.[42] The participation of this active anion in the initial reaction steps comprises the component of base catalysis in the electro-oxidation of Gly.

The glyceraldehyde generated in reactions (8) and/or (11) can chemically disintegrate in the aerated alkaline solution, and generate specific products that can also come from electrochemical reactions at the Au surface.[29, 39] However, as pointed out recently by Ide and Davis, chemical relapse of glyceraldehyde in alkaline solutions yields certain products that are not commonly observed in Au supported catalysis of Gly.[43] Therefore, it is likely that surface catalysis in this case proceeds through the interactions of a series of adsorbed intermediates. If the homogeneous reactions of base catalysis are fast compared to those of the heterogeneous surface steps, the former should not significantly interfere with the latter's detection. Furthermore, the surface-bound OH^- species has been found to play a critical role as a modifier of surface charge in (non-electrochemical) alkaline oxidation of glycerol on Au.[44] Based on these considerations, we focus here on the surface-supported reactions of Gly oxidation.

The effective n values obtained in Figs. 3 and 4 represent implicitly averaged electron numbers transferred at the spatially inhomogeneous sites across the electrode surface.[45] This averaging also extends to the voltage range of CV over which n is calculated,[46, 47] as well as to the concentration-weighted contributions of the Gly and Gly^- solution species in the initial production of glyceraldehyde.[29] Further details of this subject are discussed in the ESI. On the basis of these considerations, the n values found in Figs. 3C and 4C can be attributed to a net six-electron sequence of Gly (or glycerolate) oxidation, consecutively generating glycerate and

malonate after glyceraldehyde.[42, 48, 49] In this scheme, the reactions following the two-electron

step of eqn (8) [or eqn (11)] are:

$$C_3H_6O_3 + 3OH^- = C_3H_5O_4^- + 2H_2O + 2e^- \qquad (12)$$

$$C_3H_5O_4^- + 3OH^- = C_3H_2O_4^{2-} + 3H_2O + 2e^- \qquad (13)$$

where each step most likely follows from a combined process, as noted in the case of eqn (8),

including reaction (6) as a promoter. Accordingly, an active role of $Au(OH)_{ad}^{\delta-}$ remains implicit in

each electrochemical step of Gly/Gly$^-$ oxidation, regardless of the value of δ. The total number

of electrons released via both the routes of [(8) + (12) + (13)] and [(11) + (12) + (13)] is 6,

which is close to the (site-, voltage- and [Gly]/[Gly$^-$] concentration-averaged) value of n found

from Figs. 3 and 4.

4.4. Considerations of the rate determining step

As noted in the discussion of Figs 3 and 4, the RDS in the reaction sequence [(8) or (11) + (12)]

+ (13)] is expected to be the first dehydrogenation step,[29, 38] that is, reaction (8) or (11). Since the

RDS is the slowest process in the multi-step sequence, the irreversible attribute of the reaction

should be mostly manifested with the activation of the RDS.[50] Furthermore, the null potential of

the slow RDS is expected to be measurably different from the formal potentials (often contained

within a narrow voltage range) of the other steps in the chain.[51] If the reaction chain starts with

the RDS, according to the above considerations, the irreversible faradaic response of the

electrode should be established at a fairly low over-potential of the overall reaction and, should

subsequently remain irreversible throughout the experimental voltage range. Fig. 5 shows

illustrative results of CV experiments designed to check for this effect.

The voltammograms in Fig. 5 where collected by cycling a polycrystalline Au electrode at 50 mV s^{-1} in 2 M NaOH + 0.1 M Gly, where the upper bound of the anodic sweep was varied as follows to regulate the oxidation overpotentials: (A) 0.4, (B) 0.2 and (C) 0.0 V. The current began to rise above zero around -0.35 V, and the voltages applied more anodic to this value constituted the driving overpotentials. The lower voltage bound of these scans was kept at -1.25 V in all three cases. While strong oxidation currents were observed in the anodic scans, no corresponding reductions currents were detected in the cathodic sweeps due to the irreversible nature of the anodic reaction. As seen in Fig. 5C, this irreversible feature of the voltammogram was present even when the anodic current was activated barely above the reaction threshold, at E $= -0.35$ V. These observations were consistent with the reaction scheme based on the RDS identified as reaction (8) or (11).

The absolute tally of electrons released in the RDS of reaction (8) or (11) is two. However, the net RDS for interfacial charge transfer is formally described as a sequence of single-electron steps where the number of these steps is equal to that of the electrons involved in the RDS.[51] In this description, n_a = 1, or 0 for electrochemical or chemical reactions, respectively,[13] and accordingly, n_a = 1 for both eqns (8) and (11). The corresponding value of α given by the measured parameter $(1-\alpha)n_a$ from Figs. 3B and 4B is expected to be in the 0.83-0.89 range. Such relatively large transfer coefficients are not unusual for irreversible electrocatalytic oxidation reactions on Au electrodes.[52] In view of the results recently published by Laborda et al., this type of large values of α could arise from nonlinear solvation effects at the electro-active interface.[53]

4.5. Surface plasmon resonance as a probe of adsorbate-surface interactions at the Au film electrode

According to the mechanism of electrocatalysis discussed above, the oxidizing molecule interacts with the Au surface mostly through the active sites of $Au(OH)_{ad}^{\delta-}$.[38] Hence the overall chemisorption characteristics of the Au surface in the alkaline solution of Gly should be strongly dictated by those of $Au(OH)_{ad}^{\delta-}$ formation. Previously, the SPR technique has been shown to serve as a relatively straightforward probe of such surface specific effects.[10, 54] Therefore, an exploratory set of SPR measurements were performed for the Au film electrode used here.   Fig. 6 displays voltage dependent SPR data recorded by using the (A) Ref. and (B) Ref. + 0.1 M Gly solutions, with the Au film electrode. The sample assembly used for these measurements is described in the ESI.

Each plot in Fig. 6A and B represents the reflectance (R) of the Au-electrolyte interface as a function of the angle of optical incidence (θ) measured at the base of a light-coupling glass prism. The relatively small feature seen near the lower end of the angular scan corresponds to the critical angle (θ_c), where $\theta_c = \sin^{-1}(n_e / n_g)$, with n_e and n_g denoting the refractive indices of the electrolyte and the glass prism, respectively.[54] Since the critical angle is determined by bulk material properties, the θ_c measured from Fig. 6 remains invariant at a value of 52.80°, irrespective of the electrode potential and the electrolyte's Gly content. By using $n_g = 1.72$, along with the θ_c measured from Fig. 5A and B, we obtain $n_e = 1.37$, which represents the refractive index of the electrolyte at the applied light wavelength (635 nm from a diode laser). This shows that the low concentration Gly present in the solution does not measurably affect the refractive index of the Ref. electrolyte.[54, 55]

The main dip in $R(\theta)$, observed around the 59° angle of optical incidence in Fig. 5A and B, represents the plasmon resonance angle (θ_p). In general, θ_p is quite sensitive to variations in the electrode's interfacial properties,[21, 56] and here θ_p shifts to higher values with increasing anodic voltages. These different voltage responses of θ_c and θ_p show how the SPR signal can simultaneously detect the bulk and the interfacial effects. The potential dependent values of θ_p, measured from Fig. 6A and B are shown, respectively, by plots (a) and (b) in Fig. 6C. The line through the data points (symbols) display the general common trend of the two sets of data. The specific trend of $\theta_p(E)$ has been frequently seen in previous studies of similar SPR systems involving aqueous electrolytes,[10, 57, 58] and can be fully accounted for in terms of voltage induced variations of excess charge densities at the Au electrode surface.[10] The slight hump-like feature of the $\theta_p(E)$ plot observed around -1.0 V can be attributed to the onset of reorientation of water dipoles near the electrode's potential of zero charge.[54, 59]

The two $\theta_p(E)$ plots recorded for the Gly free and the Gly added solutions are nearly identical in Fig. 6C. This demonstrates that, regardless of the Gly content of the electrolyte, the SPR response of the Au-electrolyte interface is dominated by the intrinsic voltage dependence of the electrode's surface charge. To a large extent, this charge is governed by the surface coverages of $Au(OH)_{ad}^{\delta-}$ on Au and by the values of $\delta(E)$.[22, 60, 61] The SPR results in Fig. 6 are consistent with the mechanism of $Au(OH)_{ad}^{\delta-}$ mediated adsorption reaction of Gly considered in eqns (7) and (10): The $(OH)_{ad}^{\delta-}$ directly interacts with Au and controls the SPR angle of the Au-electrolyte interface, whereas the Gly/Gly$^-$ interacts with the $(OH)_{ad}^{\delta-}$ and introduces a relatively weaker effect in the form of a slight broadening of the SPR plots in Fig. 6B. The latter effect can

be associated with Gly/Gly⁻ induced minor changes in the imaginary dielectric function of the electrode surface layer.[10]

4.6. Voltammetric features of glycerol electro-oxidation at a rotating disc Au electrode

In view of earlier reported results for similar systems,[28] it is expected that mass transfer limited transport of reactants plays a role in restricting the anodic currents observed during the negative voltage scans in Figs. 3A and 4A. This mass transfer limitation can also hinder the progress of the multistep oxidation of Gly/Gly⁻, and hence constrain the value of n. To explore these possibilities, and to further probe the kinetic aspects of the Gly/Gly⁻ reactions on Au, a series of CV experiments were performed using a polycrystalline Au RDE. Illustrative results, collected in these experiments at a voltage scan rate of 50 mV s⁻¹, are presented in Fig. 7. Panel A displays a voltammogram recorded in the Ref. electrolyte, with ω set at 200 rpm. B shows several such plots collected in a Ref. + 0.03 M Gly electrolyte with ω varied between 150 and 900 rpm. The electrode currents detected over a given potential range are seen to increase with increasing values of ω. The Gly concentration for the RDE experiments was adjusted to 0.03 M to establish an adequate control of the limiting currents by regulating the value of ω.

The flat regions seen in the voltammograms of Fig. 7B during the anodic scans represent the limiting currents (i_L). A close-up view of these i_L sectors is shown in Fig. 7C. RDE generated cyclic voltammograms similar to those observed here have been reported in electrocatalysis studies of various alcohols.[20, 47, 62] Unlike Figs. 3 and 4, the voltammograms in Fig. 7 were recorded at a fixed scan speed; in the latter case, this has led to a cycle independent termination point for the post-peak oxidation current of Gly/Gly⁻ in the positive voltage scans. Since the disc rotation speed has minimal effects on this oxidation-stopping potential, it is

evident that the full range of ω applied here is effective for relaxing the mass transport limited faradaic response of Gly/Gly$^-$ oxidation. This is expected, because even at moderate values of ω (~100 rpm), the effects of (natural convection and) diffusion are mostly eliminated by forced convection of the RDE.[63]

The contribution of convective mass transport to the faradaic efficiency of the RDE is also seen in the higher recovery of the anodic currents generated during the reverse (cathodic) sweeps in Fig. 7B compared to those of the stationary electrode in Figs. 3A and 4A. This observation is consistent with the results reported by Qi et al., where Gly conversion on an Au/C anode was found to vary as a function of electrolyte flow rates.[64] The overall currents of Gly/Gly$^-$ oxidation in Figs. 3 and 4 are higher than those found in Fig. 7B, due to the lower Gly concentration used in the latter case.

The limiting currents observed in Fig. 7B increase with increasing values of ω according to eqn (5). However, the limiting current plateaus eventually begin to appear as "peaks" after ω exceeds a certain value (300 rpm in the present case). This effect has been frequently observed in previous CV studies of RDE systems,[65, 66] and its origin has been explained in terms of a competition between the speed of voltage scan and that of disc rotation under quasi-steady state conditions.[19, 67, 68] The underlying mechanism of this effect is briefly noted below.

The velocity component (V_x) of disc rotation along the surface normal near the electrode is expressed as: $V_x \approx -0.51(v_e^{-1/2}\omega^{3/2})x^2$, which rapidly drops to zero as $x \to 0$.[15, 67] As a result, in the close vicinity of the electrode surface, a scan rate dependent reaction zone of thickness δ_τ dominates over δ_0 as a major governing factor of the effective reaction rate.[68] Here τ denotes the timescale necessary for voltage driven replenishment of reactants at the electrode surface; $\tau = (RT / n_a Fv)$, and $\delta_\tau \approx (\pi D\tau)^{1/2}$. The value of δ_0 decreases with increasing values of ω, and

depending on the experimental system, eventually can become comparable to the dimension of δ_τ. When this happens, the voltage response of i is no longer controlled by δ_0, but is dictated by δ_τ.[67,19]

Within the reaction zone of δ_τ the interfacial characteristics of the RDE resembles those of a stationary electrode, and hence the corresponding currents become peak-shaped (as those in Figs. 3A and 4A.[68] The largely depleted reactant concentration created at the electrode interface following the anodic voltage scan is maintained in the reverse scan until the voltage reaches ~0.0 V, where the oxidation current rises again. However, owing to the continually decreasing oxidation overpotential encountered in going from −0.1 to −0.2 V, this current subsequently drops back to zero. As a result, no well-defined peaks or plateaus are detected in the cathodic voltage scans of Fig. 7B (and also in those of Figs. 3A and 4A for the same reason).

As noted above, δ_τ increases with decreasing values of v, and δ_0 decreases with increasing values of ω. Thus, the threshold of ω, at which the limiting plateau of the RDE current changes over to a peak shape, can be regulated by adjusting the value of v. In addition, according to Levich equation, the RDE current can be maintained as i_L and examined over an appreciable range of ω as long as c_b is maintained at a low/moderate value. Thus, it is necessary to simultaneously adjust the three experimental variables, v, c_b and ω in RDE based quasi steady state CV of Gly oxidation to effectively maintain the i_L plateau (this plateau is necessary for the analyses of Levich and Koutecký–Levich plots). In the present work, this has been accomplished by choosing the appropriate control variables through a series of preliminary trial measurements.

While the analysis presented in Fig. 7 is based on CV scans applied at a rate of 50 mV s^{-1}, the value of v for RDE-CV measurements is often limited in the 20-25 mV s^{-1} range.[20, 69]

Therefore, to verify the criterion of quasi-steady state, we also performed these measurements at $v = 20$ mV s^{-1} and compared the results with those recorded at 50 mV s^{-1}. For the 20 mV s^{-1} scan, the conditions necessary to support adequately widened i_L plateaus were met by using $\Omega = 80\text{-}300$ rpm, with c_b (Gly) $= 0.03$ M. As shown in Fig. 8, these additional RDE voltammograms are very similar to those obtained in Fig. 7 at $v = 50$ mV s^{-1}. This demonstrates that the quasi-steady state condition for RDE-CV is maintained in the 20-50 mV s^{-1} range of v examined here. In addition, the slower scans of CV in Fig. 8A allow for a higher recovery of the oxidation currents in the negative voltage sweeps compared to those seen in Fig. 7A. This further affirms the presence of diffusion limited (slow) transport in the eletro-oxidation of Gly.

4.7. Effects of convective mass transport on the faradaic efficiency of glycerol electro-oxidation

Fig. 9A and C displays Levich plots constructed using the anodically swept parts of RDE voltammograms collected at 50 and 20 mV s^{-1} scan rates, respectively. The corresponding plots shown in Fig. 9B and D, are based on the Koutecký-Levich equation. Due to the competing effects of ω and v mentioned in the last section, the i_L dominated sectors of the voltammogams exhibited a somewhat slanted trend at the higher rotation speeds. To confirm that these features did not arise from any voltage dependent reaction mechanisms, the i_L values were determined using standard protocols[70] at three equally spaced regions of the voltammograms between -0.05 and 0.10 V. The three plots shown in each panel of Fig. 9 correspond to the mid-point voltages of these sampling regions. As seen in the nearly coincident three plots in each panel, the voltage dependence of $i_L(\omega)$ is insignificant.

From the slopes of the linear fits to the data in Fig. 9, one can determine n by using the known values of v_e for water at 25 $^{\circ}$C, D and c_b. Since the conventional Levich (as well as the Koutecký-Levich) equation corresponds to a single step electron-transfer, the linear behavior of this equation for multistep reactions is typically observed over a limited segment of ω where the prevailing RDS dictates the reaction kinetics.[20, 71] This is seen in Fig. 9, where $\bar{n}$ indicates the average value of n collected from the three sampling voltages within the limiting current regime. These results for $\bar{n}$, obtained using two different values of v and employing the framework of both Levich and Koutecký-Levich analyses, are in close mutual agreement.

The combined average value of $\bar{n}$ obtained from the four panels of Fig. 9 is 9.31. An examination of the previously known (alkaline) reaction pathways of Gly oxidation[29, 49, 72] suggests that, the maximum expected electron count closest to this observed value of $\bar{n}$ should be 10 for the RDE system. Such a process would involve $4\,e^-$ oxidation of malonate to mesoxalate:[73]

$$C_3H_2O_4^{2-} + 4OH^- = C_3O_5^{2-} + 3H_2O + 4e^-, \tag{14}$$

occurring after reaction (13). Glyceraldehyde, malonic acid and mesoxalic acid are commonly found products of Gly oxidation on Au based electrodes, and the total 10 e$^-$ pathway detected here for reactions [(8) or (11) + (12) + (13) + (14)] is consistent with earlier published results.[5, 38, 72] The intermediates generated in the reaction sequence terminating in eqn (14) should only represent those of electron-exchanging surface reactions. Therefore, as noted in the context of eqn (11), the bulk decomposition products of glyceraldehyde do not appear to measurably interfere with the surface reactions studied here. At the same time, convective transport of electrode species (including that of OH$^-$ to the electrode surface) seems to be a critical factor for supporting reaction (14).

4.8. Rate determining step under convective mass transport

Since reaction (14) is the final step of Gly/Gly$^-$ oxidation activated here by switching from the stationary electrodes to the RDE, it is expected that the initial RDS of the reaction chain remains unchanged irrespective of the electrode's rotation. This can be verified by checking if the typical value of $n_a(1-\alpha)$, determined for the stationary electrodes (Figs. 3C and 4C), agrees with that associated with the RDE. Measuring this RDS parameter with v dependent CV, as considered in Figs. 3B and 4B, is not possible for the RDE data, because the RDE voltammograms do not use v as a control variable. Nevertheless, since the mass transfer limited component of i in Figs. 7 and 8 can be separated as i_L, these irreversible currents are suitable for Tafel analysis. In the following we evaluate $n_a(1-\alpha)$ for the RDE system using the latter approach.[20]

Figure 10 shows plots of eqn (4) using the data from Figs. 7 and 8 for the different conditions of the RDE experiments: $v = 50$ mV s^{-1}, at $\omega = 190$, 200 and 210 rpm (closed squares, circles and triangles, respectively); and $v = 20$ mV s^{-1}, at $\omega = 100$, 110 and 120 rpm (open squares, circles and triangles, respectively). All the six sets of data plotted in Fig. 10 converge on a single graph as indicated by the linear fit to the composite group. The value of $n_a(1-\alpha)$ resulting from these fits to the RDE data is 0.09, which is in general agreement with those found in Figs. 3B and 4B for the stationary electrodes. This indicates that the same RDS operates in the oxidation of Gly on both the rotating and the stationary electrodes.

5. Conclusions

The experiments reported here utilize a combination of the CV and SPR techniques to investigate the electrocatalytic steps of Gly oxidation on stationary and rotating Au electrodes in a supporting base of 2M NaOH. The cumulative number, n, of electrons released in the electro-oxidation of Gly is measured by CV with and without convective support for mass transport. These values of n are used as markers of the associated surface reactions to identify the step-wise generated electro-oxidation products of Gly. The kinetic features of the voltammetric data are examined by varying the potential sweep rates of stationary Au electrodes, and by varying the disc rotation speeds of an Au RDE.

The effective n values measured for the stationary Au electrodes are indicative of a 6 e^- oxidation process for both Gly and Gly^-, where the latter solution species comes from the base catalysis of Gly. The experimentally monitored electron-counts suggest glyceraldehyde, glycerate and malonate as the subsequent oxidation products of Gly/Gly^-. At the stationary electrode surface, this oxidation sequence terminates at the six-electron stage due to diffusion limitation of reactants and site blocking. Controlled variations of the upper voltage bound of CV scans indicate that the initial dehydrogenation of Gly/Gly^- is the RDS. Levich and Koutecký-Levich analyses of the RDE data suggest a 10 e^- process for the RDE. The increased electron yield found for the RDE is attributed to further oxidation of malonate to mesoxalate (4 e^-). Tafel plots obtained from the RDE-CV data demonstrate that, the RDS of Gly/Gly- oxidation remains unchanged between the stationary and rotating electrodes.

While the initial base catalysis of Gly is controlled by bulk OH^- species, the surface bound $(OH)_{ad}$ facilitate the successive oxidation steps of Gly/Gly^-. The $(OH)_{ad}$ surface species acts as a coupler between the Au surface and the co-adsorbing Gly species, where the activation

26

barrier for the latter's oxidation is lowered. Thus the chemisorption characteristics of the Au surface within the oxidation regime of Gly continue to be dominated by those of OH^-. This role of the surface bound OH is verified with SPR measurements performed within the voltage region of Gly oxidation.

References

1. A. N. Geraldes, D. F. Silva, J. C. M. Silva, R. F. B. Souza, E. V. Spinacé, A. O. Neto, M. Linardi and M. C. Santos, *J. Brazilian Chem. Soc.*, 2014, 25, 831-840.
2. N. Dimitratos, J. A. Lopez-Sanchez, J. M. Anthonykutty, G. Brett, A. F. Carley, R. C. Tiruvalam, A. A. Herzing, C. J. Kiely, D. W. Knight and G. J. Hutchings, *Phys. Chem. Chem. Phys.*, 2009, 11, 4952-4961.
3. Y. Shen, Z. Zhang, K. Xiao and J. Xi, *Phys. Chem. Chem. Phys.*, 2014, 16, 21609-21614.
4. J.-h. Zhang, Y.-j. Liang, N. Li, Z.-y. Li, C.-w. Xu and S. P. Jiang, *Electrochim. Acta*, 2012, 59, 156-159.
5. Z. Zhang, L. Xin and W. Li, *Int. J. Hydrog. Energy*, 2012, 37, 9393-9401.
6. L. D. Burke, J. F. Healy, K. J. O'Dwyer and W. A. O'Leary, *J. Electrochem. Soc.*, 1989, 136, 1015-1021.
7. L. D. Burke, *Electrochim. Acta*, 1994, 39, 1841-1848.
8. R. L. Doyle, I. J. Godwin, M. P. Brandon and M. E. G. Lyons, *Phys. Chem. Chem. Phys.*, 2013, 15, 13737-13783.
9. B. Lertanantawong, A. P. O'Mullane, W. Surareungchai, M. Somasundrum, L. D. Burke and A. M. Bond, *Langmuir*, 2008, 24, 2856-2868.
10. K. A. Assiongbon and D. Roy, *Surf. Sci.*, 2005, 594, 99-119.
11. A. P. O'Mullane, S. J. Ippolito, Y. M. Sabri, V. Bansal and S. K. Bhargava, *Langmuir*, 2009, 25, 3845-3852.
12. R. Parsons, *Trans. Faraday Society*, 1951, 47, 1332-1344.
13. S. Fletcher, *J. Solid State Electrochem.*, 2009, 13, 537-549.
14. A. K. N. R. J. O'M. Bockris, M. E. Gamboa-Aldeco, *Modern Electrochemistry 2A: Fundamentals of Electrodics*, Plenum Press, New York, 2001.
15. L. R. F. Allen J. Bard, *Electrochemical Methods Fundamentals and Applications*, John Wiley & Sons, New York, 2001.
16. R. S. Nicholson and I. Shain, *Anal. Chem.*, 1964, 36, 706-723.
17. D. M. F. Santos and C. A. C. Sequeira, *Electrochim. Acta*, 2010, 55, 6775-6781.
18. J. Hou, M. W. Ellis and R. B. Moore, *Electrochem. Solid-State Lett.*, 2012, 15, B39-B43.
19. P. C. Andricacos and H. Y. Cheh, *J. Electrochem. Soc.*, 1980, 127, 2385-2388.
20. D. A. Finkelstein, N. D. Mota, J. L. Cohen and H. D. Abruña, *J. Phys. Chem. C*, 2009, 113, 19700-19712.
21. C. M. Pettit, K. A. Assiongbon, J. E. Garland and D. Roy, *Sens. Actuator B*, 2003, 96, 105-113.
22. M. J. Walters, J. E. Garland, C. M. Pettit, D. S. Zimmerman, D. R. Marr and D. Roy, *J. Electroanal. Chem.*, 2001, 499, 48-60.

23.   U. Oesch and J. Janata, *Electrochim. Acta*, 1983, 28, 1237-1246.
24.   J. S. Gordon and D. C. Johnson, *J. Electroanal. Chem.*, 1994, 365, 267-274.
25.   S. Srinivasan and E. Gileadi, *Electrochim. Acta*, 1966, 11, 321-335.
26.   D. W. Kirk, F. R. Foulkes and W. F. Graydon, *J. Electrochem. Soc.*, 1980, 127, 1069-1076.
27.   J. Vancea, G. Reiss, F. Schneider, K. Bauer and H. Hoffmann, *Surf. Sci.*, 1989, 218, 108-126.
28.   J. Hernández, J. Solla-Gullón, E. Herrero, A. Aldaz and J. M. Feliu, *Electrochim. Acta*, 2006, 52, 1662-1669.
29.   Y. Kwon, K. J. P. Schouten and M. T. M. Koper, *ChemCatChem*, 2011, 3, 1176-1185.
30.   P. X.-Y. Li Qiang, *Acta Phys. Sinica*, 2013, 62, 094206.
31.   Z.-P. Liu, P. Hu and A. Alavi, *J. Amer. Chem. Soc.*, 2002, 124, 14770-14779.
32.   A. M. Nowicka, U. Hasse, G. Sievers, M. Donten, Z. Stojek, S. Fletcher and F. Scholz, *Angew. Chem. Int. Ed.*, 2010, 49, 3006-3009.
33.   B. J. Plowman, A. P. O'Mullane and S. K. Bhargava, *Faraday Discussions*, 2011, 152, 43-62.
34.   P. Rodriguez, Y. Kwon and M. T. M. Koper, *Nat Chem*, 2012, 4, 177-182.
35.   A. Chen and J. Lipkowski, *J. Phys. Chem. B*, 1999, 103, 682-691.
36.   T. Mallat and A. Baiker, *Chem. Rev.*, 2004, 104, 3037-3058.
37.   O. Enea and J. P. Ango, *Electrochim. Acta*, 1989, 34, 391-397.
38.   M. L. Avramov-Ivić, J. M. Leger, C. Lamy, V. D. Jović and S. D. Petrović, *J. Electroanal. Chem.*, 1991, 308, 309-317.
39.   Y. Kwon, S. C. S. Lai, P. Rodriguez and M. T. M. Koper, *J. Amer.Chem. Soc.*, 2011, 133, 6914-6917.
40.   B. N. Zope, D. D. Hibbitts, M. Neurock and R. J. Davis, *Science*, 2010, 330, 74-78.
41.   H. C. B. Hansen and R. M. Taylor, *Clay Minerals*, 1991, 26, 311-327.
42.   L. Xin, Z. Zhang, Z. Wang and W. Li, *ChemCatChem*, 2012, 4, 1105-1114.
43.   M. S. Ide and R. J. Davis, *Acc. Chem. Res.*, 2013, 47, 825-833.
44.   K. N. Heck, B. G. Janesko, G. E. Scuseria, N. J. Halas and M. S. Wong, *ACS Catalysis*, 2013, 3, 2430-2435.
45.   M. D. Levi, N. V. Fedorovich and B. B. Damaskin, *Canadian J. Chem.*, 1981, 59, 2019-2025.
46.   J. W. Schultze and K. J. Vetter, *J. Electroanal. Chem.*, 1973, 44, 63-81.
47.   G. Hou, J. Parrondo, V. Ramani and J. Prakash, *J. Electrochem. Soc.*, 2014, 161, F252-F258.
48.   S. Carrettin, P. McMorn, P. Johnston, K. Griffin and G. J. Hutchings, *Chem. Commun.*, 2002, 7, 696-697.
49.   J. Gomes and G. Tremiliosi-Filho, *Electrocatal*, 2011, 2, 96-105.
50.   G. H. F.G. Thomas, *Introduction to Voltammetric Analysis - Theory and Practice*, CSIRO Publishing Collingwood, 2001.
51.   J. O. M. Bockris and Z. Nagy, *J. Chem. Edu.*, 1973, 50, 839.
52.   G. Rostamikia, A. J. Mendoza, M. A. Hickner and M. J. Janik, *J. Power Sources*, 2011, 196, 9228-9237.
53.   E. Laborda, M. C. Henstridge and R. G. Compton, *J. Electroanal. Chem.*, 2012, 681, 96-102.

Physical Chemistry Chemical Physics Accepted Manuscript

54.   C. M. Sulyma, C. M. Pettit, J. E. Garland and D. Roy, *Surf. Interface Anal.*, 2012, 44, 801-810.
55.   D. Roy, *Opt. Commun.*, 2001, 200, 119-130.
56.   D. Roy and J. Fendler, *Adv. Mater.*, 2004, 16, 479-508.
57.   J. E. Garland, K. A. Assiongbon, C. M. Pettit and D. Roy, *Anal. Chim. Acta*, 2003, 475, 47-58.
58.   R. J. Heaton, A. W. Peterson and R. M. Georgiadis, *Proc. National Acad. Sci.*, 2001, 98, 3701-3704.
59.   Z. D. Schultz, S. K. Shaw and A. A. Gewirth, *J. Amer. Chem. Soc.*, 2005, 127, 15916-15922.
60.   C. M. Pettit, P. C. Goonetilleke, C. M. Sulyma and D. Roy, *Anal. Chem.*, 2006, 78, 3723-3729.
61.   C. M. Pettit, M. J. Walters and D. Roy, *Laser Chem.*, 2002, 20, 57-79.
62.   P. Rodriguez and M. T. M. Koper, *PCCP Phys. Chem. Chem. Phys.*, 2014, 16, 13583-13594.
63.   N. P. C. Stevens, M. B. Rooney, A. M. Bond and S. W. Feldberg, *J. Phys. Chem. A*, 2001, 105, 9085-9093.
64.   J. Qi, L. Xin, D. J. Chadderdon, Y. Qiu, Y. Jiang, N. Benipal, C. Liang and W. Li, *Appl. Catalysis B*, 2014, 154–155, 360-368.
65.   L. A. Diaz, A. Valenzuela-Muñiz, M. Muthuvel and G. G. Botte, *Electrochim. Acta*, 2013, 89, 413-421.
66.   R. Jiang and S. Dong, *J. Electroanal. Chem.*, 1990, 291, 11-22.
67.   J. Strutwolf and W. W. Schoeller, *Electroanalysis*, 1996, 8, 1034-1039.
68.   I. Fried and P. J. Elving, *Anal. Chem.*, 1965, 37, 803-806.
69.   G. Hou and J. Prakash, *ECS Transactions*, 2006, 1, 27-33.
70.   C. Ponce-de-León, C. T. J. Low, G. Kear and F. C. Walsh, *J. Appl. Electrochem.*, 2007, 37, 1261-1270.
71.   S. Treimer, A. Tang and D. C. Johnson, *Electroanal.*, 2002, 14, 165-171.
72.   Z. Zhang, L. Xin and W. Li, *Appl. Catalysis B*, 2012, 119–120, 40-48.
73.   N. Dimitratos, A. Villa, C. L. Bianchi, L. Prati and M. Makkee, *Appl. Catalysis A*, 2006, 311, 185-192.

Figure Captions

Figure 1. (A) Voltammograms for a gold film electrode recorded using CV in 2 M NaOH at a scan rate of 0.05 V s^{-1}. (B) Voltammograms of the Au film electrode obtained in 2 M NaOH using different scan speeds between 0.03 (inner most plot) and 1 V s^{-1} (outer most plot). The potentials (E_p) corresponding to the (a) anodic and (b) cathodic current peaks are shown in (C). (D) Shows voltage scan rate dependent peak valuess (i_p) of the (a) anodic and (b) cathodic currents taken from (B). In (C) and (D), the symbols denote data points and the traces are linear fits to the data.

Figure 2. CV data for a polycrystalline Au stationary electrode, recorded in 2M NaOH using (A) v = 0.05 V s^{-1}, and (B) at different values of v between 0.03 and 1 V s^{-1}. The anodic potential

(E_P) and the current densities (i_p) corresponding to the peaks found in (B) are also shown as of functions (C) log (v) and (D) v, respectively; the traces are fits to the data (symbols).

Figure 3. (A) CV data for a gold film electrode collected in 2 M NaOH + 0.1 M Gly at different scan rates between 0.03 and 1.0 V s^{-1}. The inset in (A) separately shows the currents from the positive voltage scans. The potentials (E_P) and the electrode currents (i_p) corresponding to the anodic peaks are shown as functions of (B) log (v) and (C) v, respectively; ; the traces are fits to the data (symbols).

Figure 4 (A) CV data for a polycrystalline Au stationary electrode, recorded in 2M NaOH + 0.1M Gly at different scan rates between 0.03 and 1.0 V s^{-1}. The inset in (A) separately shows the currents from the positive voltage scans. The potentials (E_P) and the electrode currents (i_p) found at the peak points of the graphs in (A) are shown as functions of v in (B) and (C), respectively. The symbols and the traces denote experimental data and linear fits to the data, respectively (B and C).

Figure 5. Currents of Gly electro-oxidation at the surface of a stationary polycrystalline Au electrode, varied as a function of the maximum anodic overpotential applied. The arrows indicate the direction of voltage scan.

Figure 6. Angle resolved SPR reflectivity plots (A and B) for a thin film Au electrode, recorded at different voltages in 0.1 V intervals between −0.5 and 0.5 V using 2 M NaOH + x M Gly electrolytes. (C) Voltage dependent SPR angles (θ_p), taken from A (squares) and B (circles). The symbols are experimental data and the solid line shows the common general trend of the data for both values of x.

Figure 7. (A) CV data for a gold RDE, recorded in (A) 2M NaOH and (B) 2 M NaOH + 0.03 M Gly at a voltage scan rate of 0.05 V s^{-1}. The electrode rotation speed is 200 rpm in (A) and varied between 150 and 900 rpm in (B). The limiting current regions of the voltammograms observed during the anodic sweeps in (B) are separately shown in (C).

Figure 8. (A) CV data for a gold RDE, recorded in 2M NaOH + 0.03 M Gly at a voltage scan rate of 20 mV s^{-1}, with ω varied as shown. The limiting current regions of the voltammograms observed during the anodic sweeps in (A) are separately shown in (B).

Figure 9. (A) Levich and (B) Koutecký-Levich plots of the limiting current for a gold RDE, recorded at v = 0.05 V s^{-1}. The traces are linear fits to the appropriate regions of the data (ω < 300 rpm). (C) and (D) show, respectively, Levich and Koutecký Levich graphs obtained for the Au RDE at v = 0.02 V s^{-1}. The linear fits to the data in (C) and (D) correspond to ω < 180 rpm.

Figure 10. Tafel plots for the Au polycrystalline RDE, recorded in 2 M NaOH with 0.03 M Gly using two different rates of voltage sweep (mV s^{-1}) at several angular speeds of disc rotation (rpm). A single linear fit is applied to the full data set.
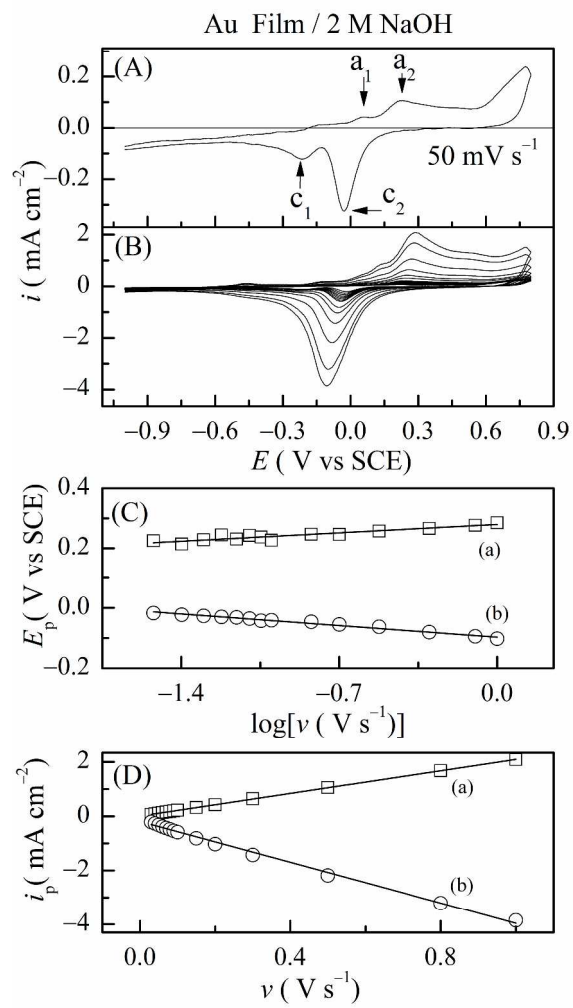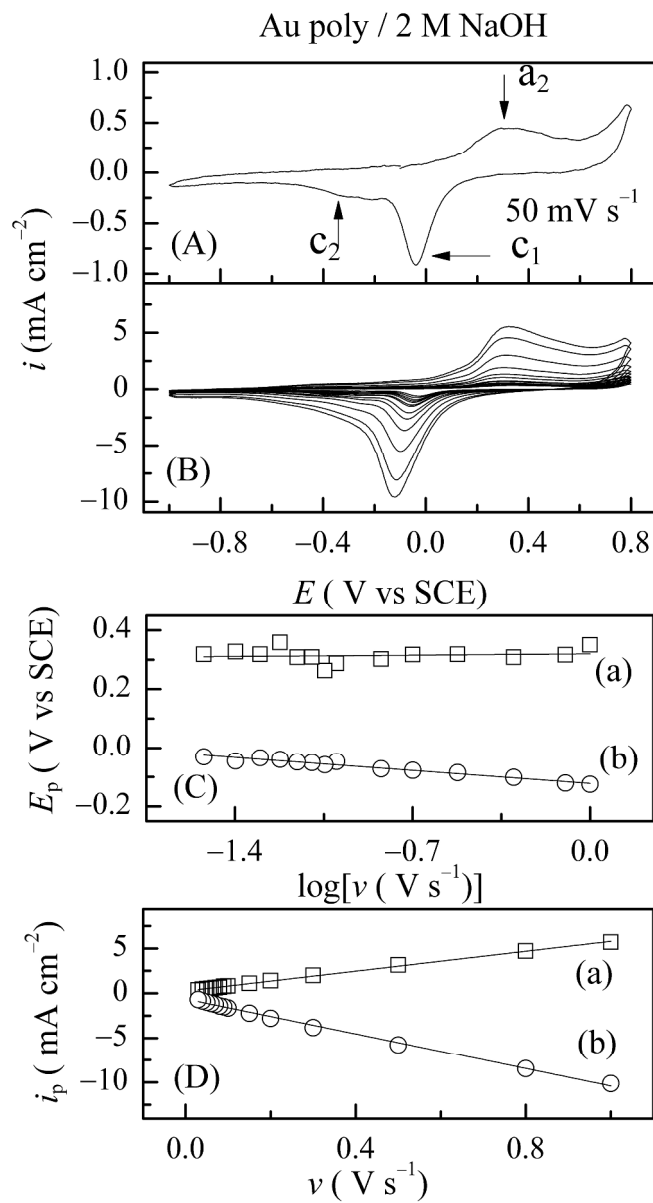
Fig 1
304x609mm (300 x 300 DPI)

Au poly / 2 M NaOH

Fig 2
251x458mm (300 x 300 DPI)
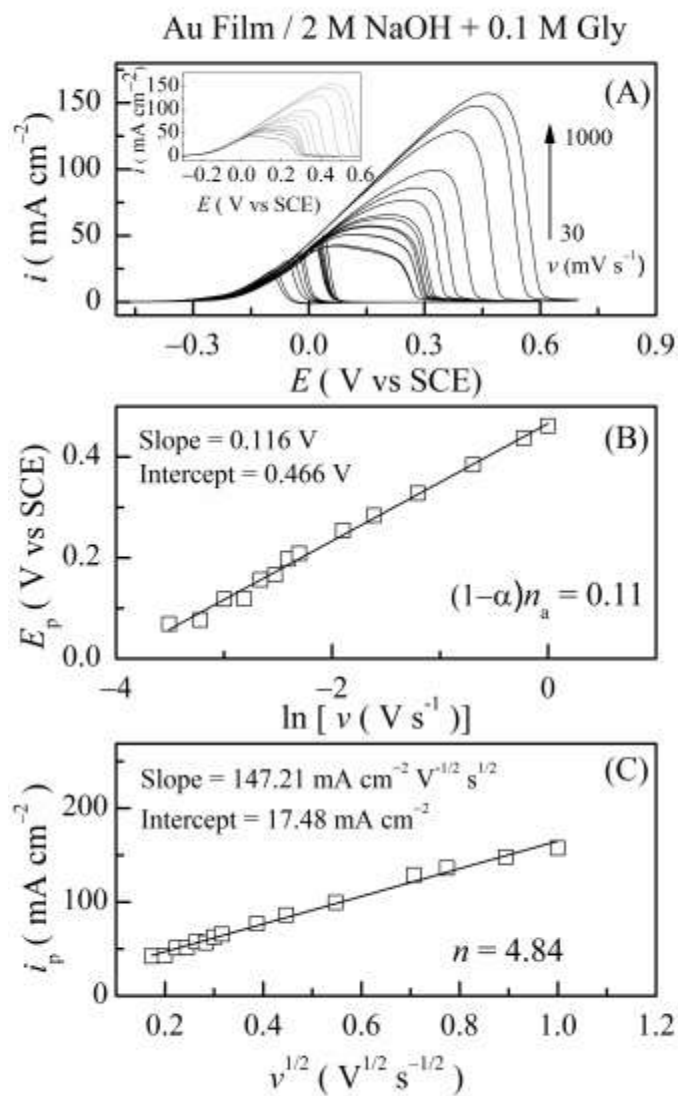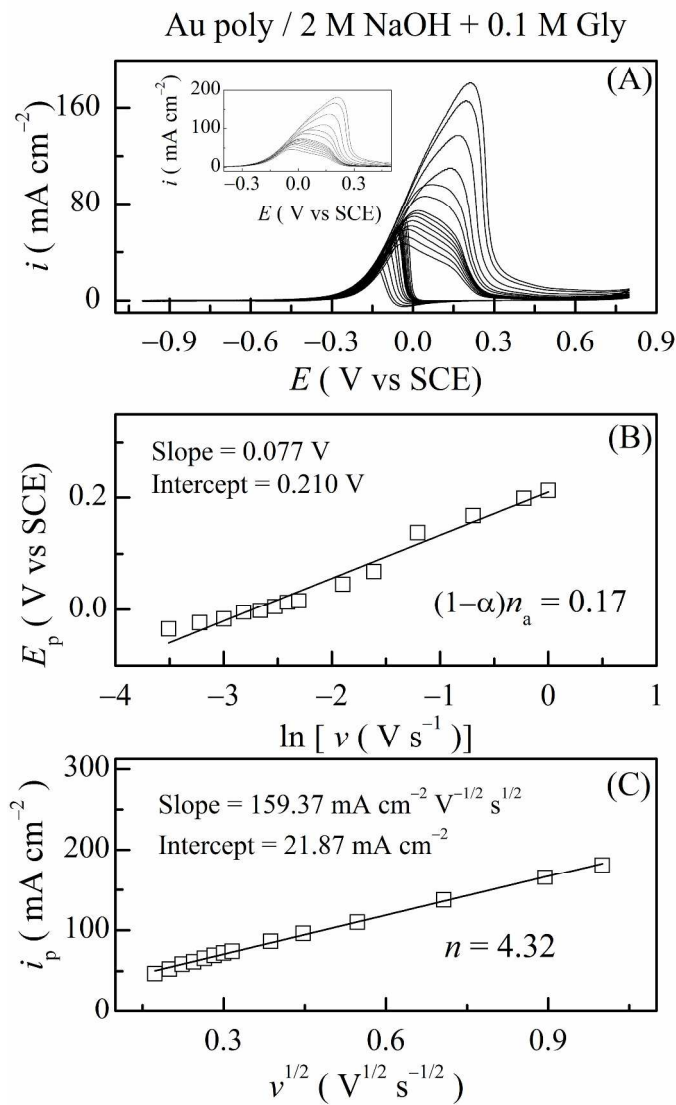
Au Film / 2 M NaOH + 0.1 M Gly

Fig 3
254x423mm (300 x 300 DPI)

Fig 4
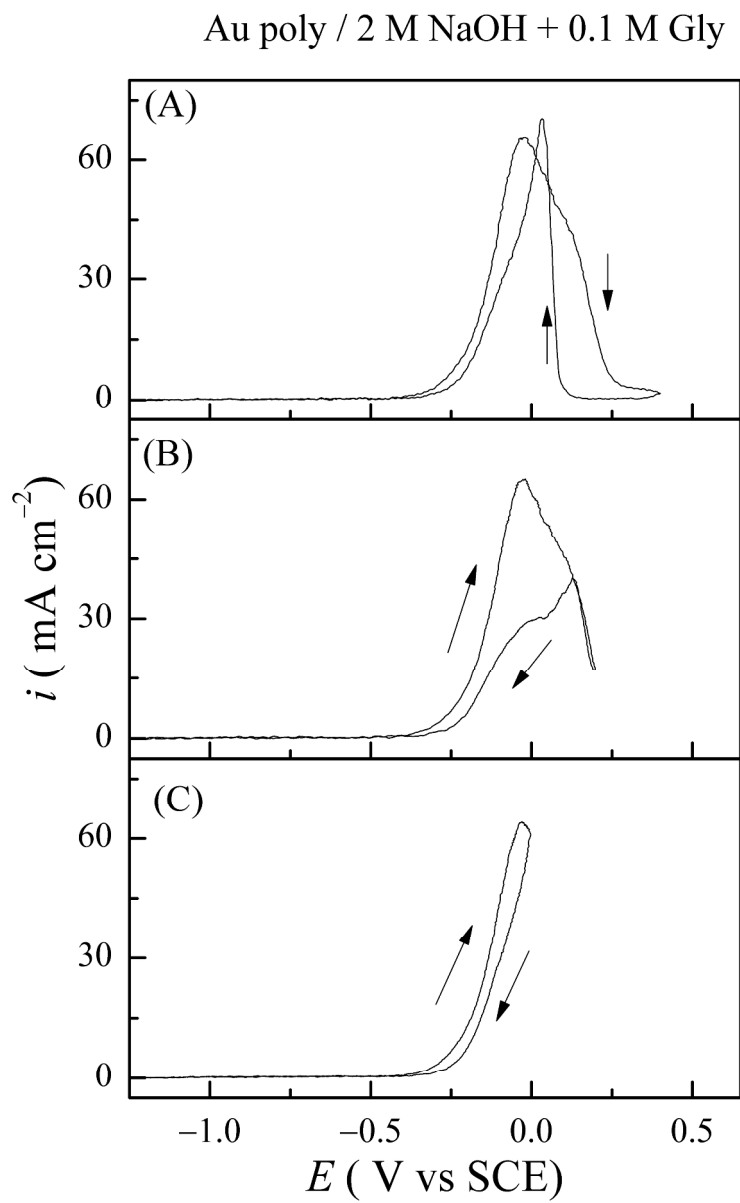254x423mm (300 x 300 DPI)

Fig 5
224x363mm (300 x 300 DPI)

Au Film / 2 M NaOH + x M Gly

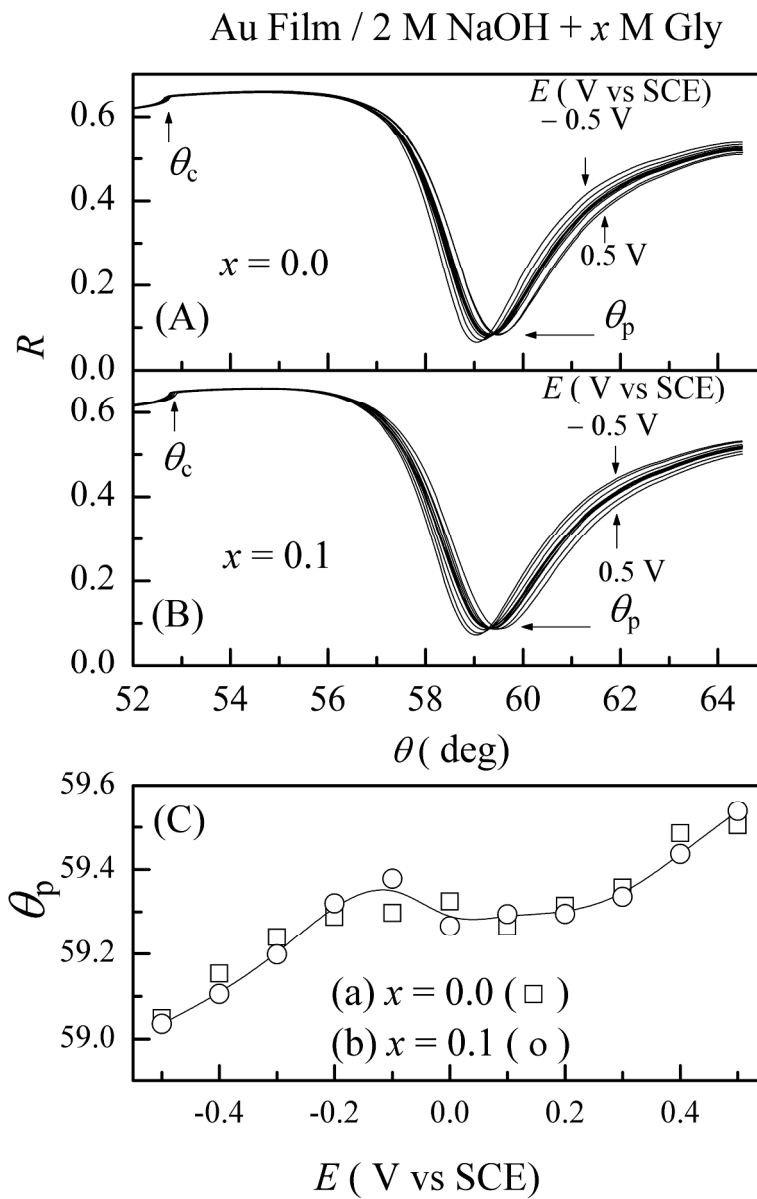Fig 6
216x332mm (300 x 300 DPI)
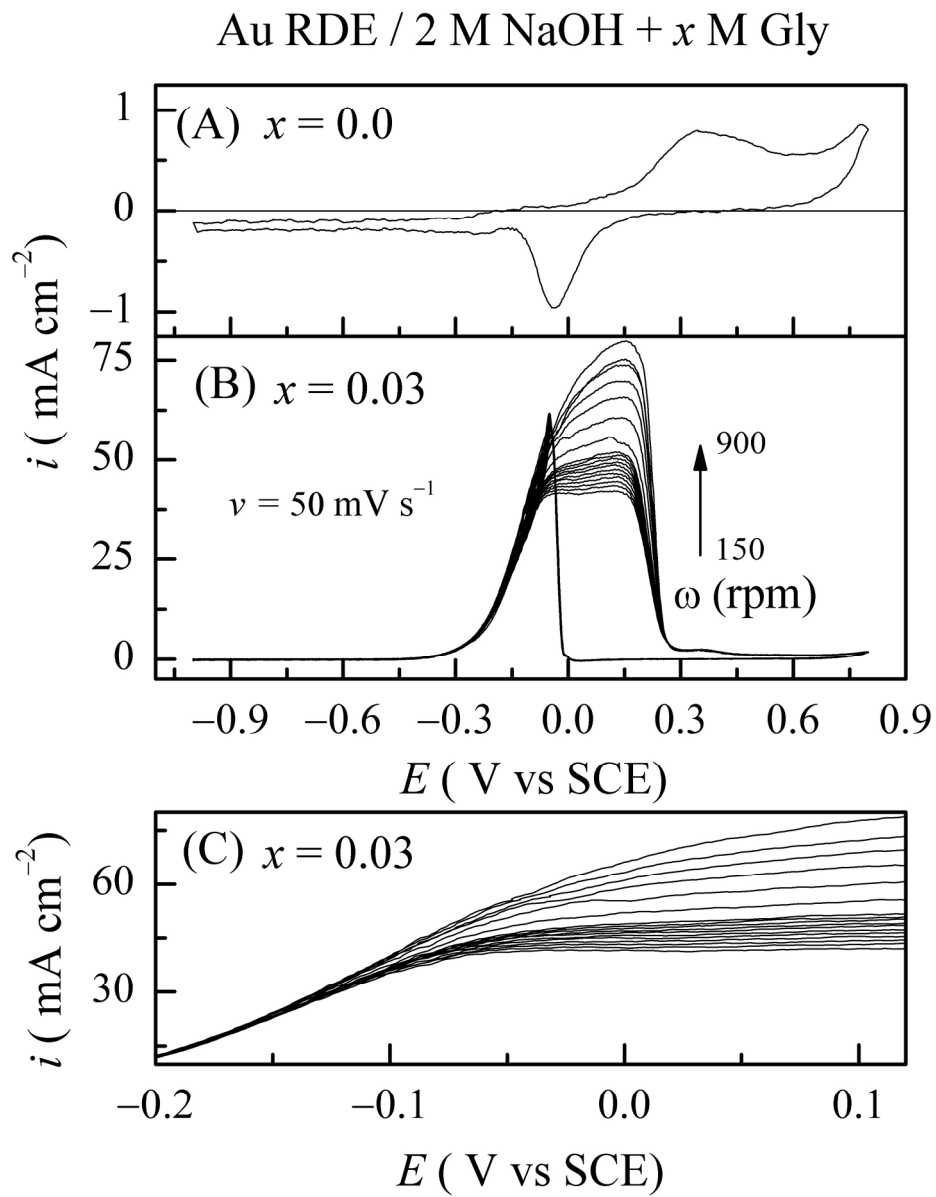
Fig 7
183x231mm (300 x 300 DPI)

Au RDE / 2 M NaOH + 0.03 M Gly

(A)

$v = 20\ mV\ s^{-1}$

300

80

ω (rpm)

E (V vs SCE)
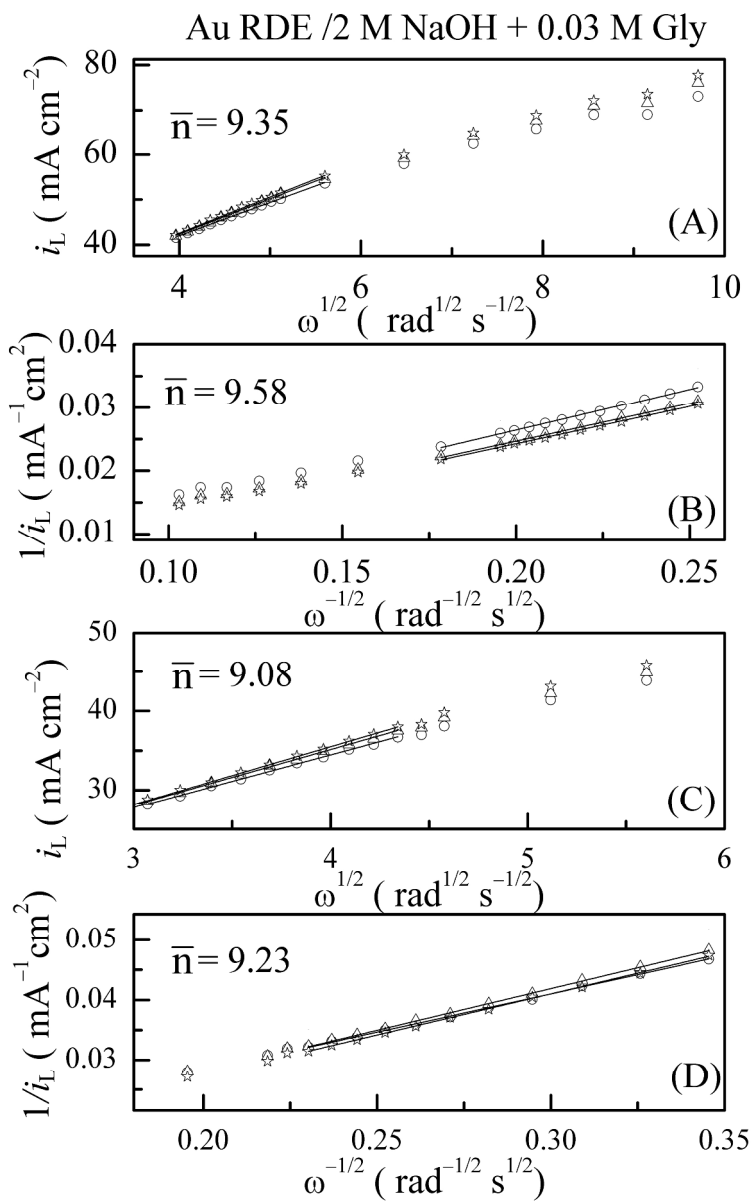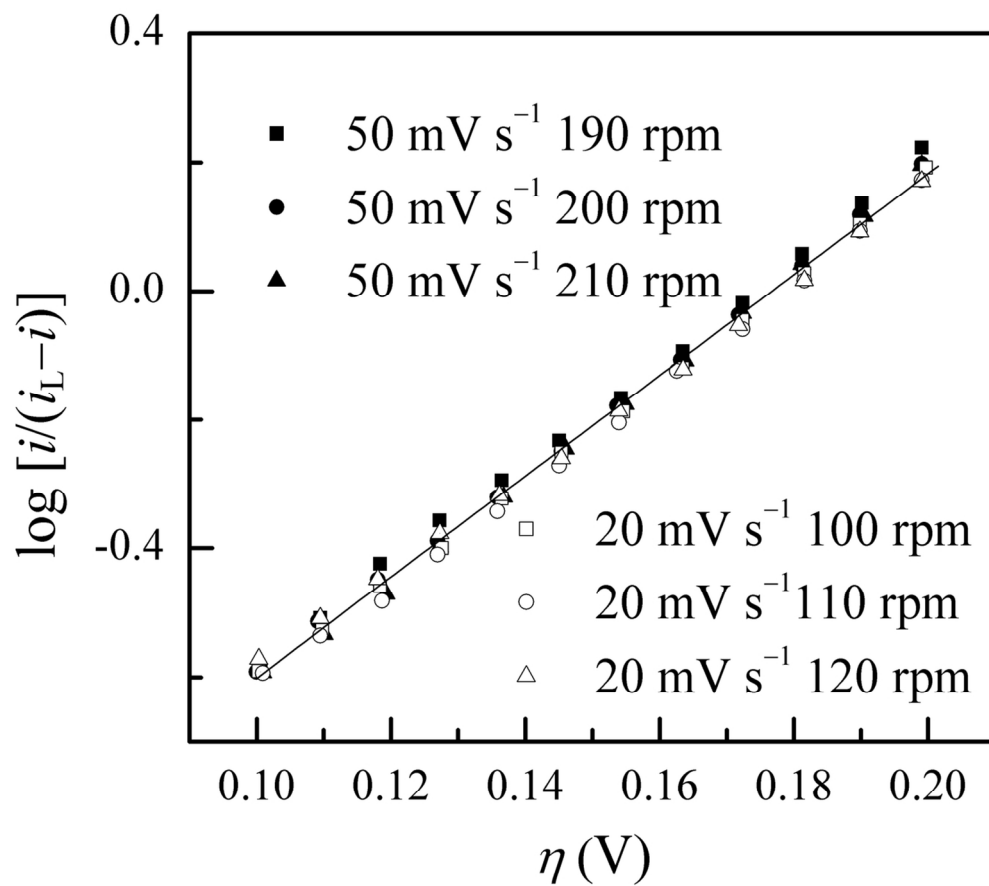
(B)

E (V vs SCE)
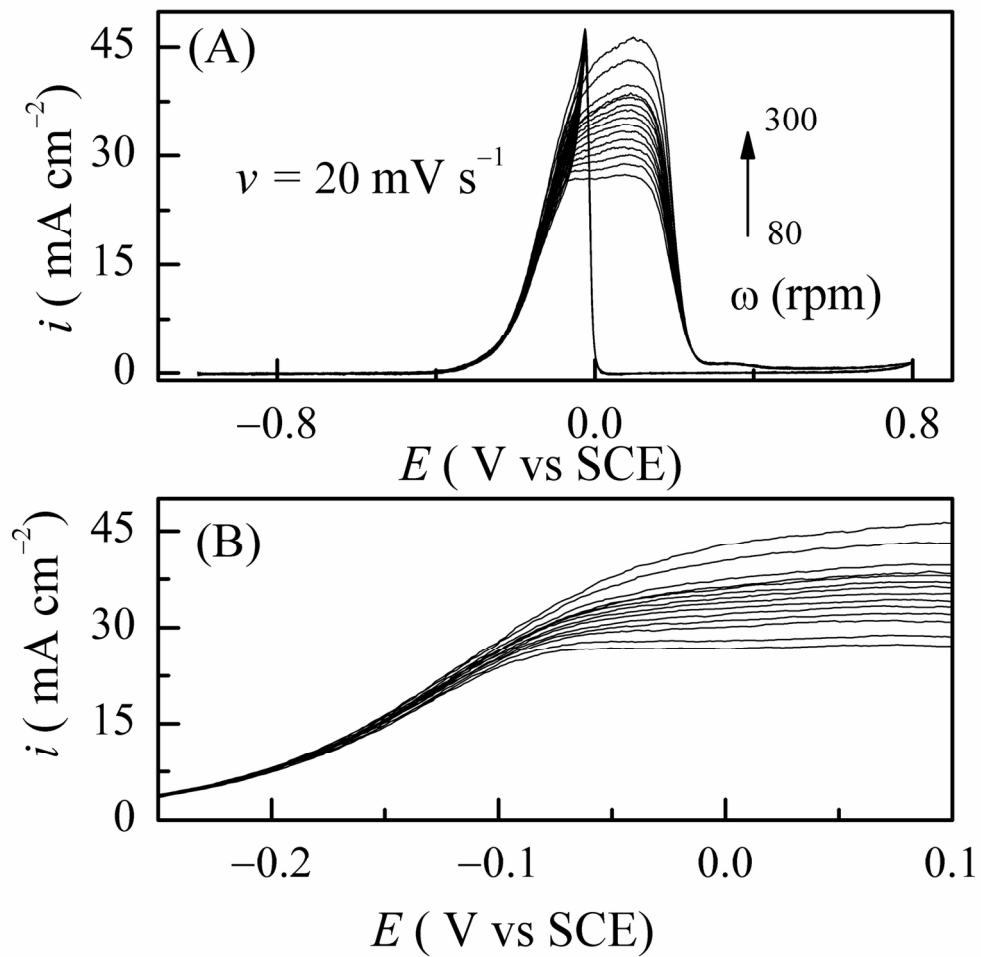
Fig 8
150x157mm (300 x 300 DPI)

Fig 9
232x369mm (300 x 300 DPI)

Fig 10
115x102mm (300 x 300 DPI)